Internal-magnetic-field distribution at the critical current of a type-II superconductor subjected to a parallel magnetic field

John R. Clem and Antonio Perez-Gonzalez*
Ames Laboratory—U.S. Department of Energy and Department of Physics, Iowa State University, Ames, Iowa 50011
(Received 1 August 1985)

A general critical-state model including the effects of both flux-line cutting and flux pinning is used to predict the internal-magnetic-field distribution at the critical current of type-II superconductors subjected to parallel magnetic fields. The anticipated behavior is considered for specimens in the form of both slabs or strips and thin-walled cylindrical shells. Striking dependences upon the applied field angle are predicted for the direction of the electric field in slab geometry and for the magnitude and direction of the induced azimuthal current in cylindrical geometry.

I. INTRODUCTION

The internal-magnetic-field distribution just above the critical current of a type-II superconductor in a parallel applied magnetic field has long been a puzzling problem[1] and still is a subject of controversy.[2–47] Recently, we have developed a macroscopic theory[16–18,36–38] to treat the related problem of the hysteretic response of a type-II superconducting slab subjected to a parallel magnetic field that varies in both magnitude and direction. The theory, which was motivated by the experiments and the empirical models suggested in Refs. 10, 28, 29, and 48–59, takes the form of a general critical-state model. This model includes not only the effects of flux pinning, as in the usual critical-state model,[60–62] but also the effects of flux-line cutting.[62,63] Flux-line cutting (intersection and cross joining of adjacent nonparallel vortices) is the quantum analog in the superconducting state of magnetic reconnection,[64] which produces numerous phenomena in astrophysical plasmas. There is evidence that the corresponding effect also occurs in superfluid ^{4}He, where the process is called vortex-line reconnection.[65,66] In the present paper, we show how our general critical-state theory can be used to predict the unique time-independent macroscopic magnetic field distribution that should accompany the constant macroscopic electric field just above the critical current of a type-II superconductor in a parallel applied magnetic field. For simplicity, we limit our attention to specimens in the form of either slabs (strips) or thin-walled cylindrical shells.

In Sec. II we give the basic equations of the critical-state theory. This theory is applied to slab geometry in Sec. III and to cylindrical geometry in Sec. IV. Finally, we summarize and discuss our results in Sec. V.

II. BASIC THEORY

Consider a high-κ, irreversible type-II superconducting infinite slab of thickness $X=2x_m$. Applied to the surfaces $x=0$ and $x=X$ are parallel magnetic fields $\mathbf{B}_{s0}=B_{s0}\hat{\mathbf{a}}_{s0}$ and $\mathbf{B}_{sX}=B_{sX}\hat{\mathbf{a}}_{sX}$, where $B_s=|\mathbf{B}_s|$ and

$$\hat{\mathbf{a}}_s=\hat{\mathbf{y}}\sin\alpha_s+\hat{\mathbf{z}}\cos\alpha_s\ . \tag{1}$$

The fields $\mathbf{B}_{s0}$ and $\mathbf{B}_{sX}$ are comprised of not only the applied field but also the self-field generated by a transport current flowing in the slab. We assume that to good approximation $\mathbf{B}=\mu_0\mathbf{H}$ inside the sample, and we neglect any surface barriers against vortex entry or exit. We further assume that in steady state the magnetic induction $\mathbf{B}$ inside the sample is independent of time and depends only upon the coordinate x; i.e., $\mathbf{B}(x)=B(x)\hat{\mathbf{a}}(x)$, where $B=|\mathbf{B}|$ and

$$\hat{\mathbf{a}}=\hat{\mathbf{y}}\sin\alpha+\hat{\mathbf{z}}\cos\alpha\ . \tag{2}$$

The surface boundary conditions on $\mathbf{B}$ are $\mathbf{B}(0)=\mathbf{B}_{s0}$ and $\mathbf{B}(X)=\mathbf{B}_{sX}$.

In steady state, Ampere's law, $\mathbf{J}=\nabla\times\mathbf{H}$, dictates that the differences in B_y and B_z across the slab be determined by the average current density components $\bar{J}_z$ and $\bar{J}_y$, respectively:

$$\Delta B_y=B_{sXy}-B_{s0y}=\mu_0\bar{J}_zX\ , \tag{3}$$

$$\Delta B_z=B_{sXz}-B_{s0z}=-\mu_0\bar{J}_yX\ . \tag{4}$$

Similarly, in steady state, Faraday's law, $\nabla\times\mathbf{E}=\mathbf{0}$, dictates that $\mathbf{E}=\mathbf{E}_0$, a constant independent of x.

Resolving the current density $\mathbf{J}(x)$ and the electric field $\mathbf{E}$ into their components parallel and perpendicular to the local $\mathbf{B}$ (i.e., writing $\mathbf{J}=J_{\parallel}\hat{\mathbf{a}}+J_{\perp}\hat{\boldsymbol{\beta}}$ and $\mathbf{E}=E_{\parallel}\hat{\mathbf{a}}+E_{\perp}\hat{\boldsymbol{\beta}}$, where $\hat{\boldsymbol{\beta}}=\hat{\mathbf{a}}\times\hat{\mathbf{x}}$), we obtain from Ampere's and Faraday's laws in steady state

$$J_{\parallel}=\mu_0^{-1}B\frac{\partial\alpha}{\partial x}\ , \tag{5}$$

$$J_{\perp}=-\mu_0^{-1}\frac{\partial B}{\partial x}\ , \tag{6}$$

and

$$E_{\parallel}\frac{\partial\alpha}{\partial x}+\frac{\partial E_{\perp}}{\partial x}=0\ , \tag{7}$$

$$E_{\perp}\frac{\partial\alpha}{\partial x}-\frac{\partial E_{\parallel}}{\partial x}=0\ . \tag{8}$$

As discussed in Refs. 16–18 and 36–38, a nonvanishing $E_{\perp}$ can occur only where the magnitude of $J_{\perp}$ is

larger than $J_{c\perp}(B)$, the transverse critical-current density at the threshold for depinning of the vortex array, and a nonvanishing $E_{\parallel}$ can occur only where the magnitude of $J_{\parallel}$ is larger than $J_{c\parallel}(B)$, the parallel critical-current density at the threshold for flux-line cutting in the vortex array. We assume that the pinning properties are isotropic, such that $J_{c\perp}$ and $J_{c\parallel}$ depend upon the magnitude of $\mathbf{B}$ but not upon its angle relative to some symmetry direction in the specimen.

Above the critical current of the slab, where $E_0 \neq 0$, Eqs. (7) and (8) reveal that at some coordinate x either (a) both $E_{\parallel}$ and $E_{\perp}$ are nonzero, such that x is in a CT (cutting-transport) zone where both cutting and transport are occurring, or (b) only $E_{\perp}$ is nonzero, such that x is in a T zone where only transport is occurring. For the latter case, each vortex keeps the same angle relative to the specimen as it moves toward regions of smaller B. Note that, because $E_{\parallel}$ can be nonzero only when $\partial\alpha/\partial x$ is nonzero, Eq. (7) excludes the possibility of a C zone in steady state, where $E_{\parallel} \neq 0$ and $E_{\perp}=0$, such that flux-line cutting would occur without flux transport.

We consider the behavior just above the critical current, where we assume that

$$E_{\perp}=\rho_{\perp}(J_{\perp} \mp J_{c\perp}) \tag{9}$$

when $E_{\perp} \gtrless 0$ and

$$E_{\parallel}=\rho_{\parallel}(J_{\parallel} \mp J_{c\parallel}) \tag{10}$$

when $E_{\parallel} \gtrless 0$. Here, $\rho_{\perp}$ and $\rho_{\parallel}$ are effective flux-flow and flux-cutting resistivities of the material. Because we assume here that $|E_{\perp}| \ll \rho_{\perp} J_{c\perp}$ and $|E_{\parallel}| \ll \rho_{\parallel} J_{c\parallel}$, the distributions of $\mathbf{B}$ computed in Secs. III and IV are independent of $\rho_{\perp}$ and $\rho_{\parallel}$.

For simplicity, we consider only sufficiently thin slabs that the magnitude of the self-field at the critical current is a small fraction of the total B in the slab. This guarantees that $\mu_0|\bar{J}_z|X \ll \bar{B}$, $\mu_0|\bar{J}_y|X \ll \bar{B}$, $|B(x)-\bar{B}|/\bar{B} \ll 1$, and $|\alpha(x)-\bar{\alpha}| \ll 1$, where $\bar{B}$ and $\bar{\alpha}$ are the averages of B and α over the slab thickness. With the assumption that $J_{c\perp}(B)$ and $J_{c\parallel}(B)$ vary smoothly with B, we can safely treat $J_{c\perp}$ and $J_{c\parallel}$ as constants; i.e., we take $J_{c\perp}=J_{c\perp}(\bar{B})$ and $J_{c\parallel}=J_{c\parallel}(\bar{B})$.

In the following sections, we use the above formalism to determine the distribution of $\mathbf{B}$ in two different geometries. In Sec. III we consider a slab or strip, but the results also apply to a thin-walled cylindrical shell with a slit along its length. In Sec. IV we consider a cylindrical shell.

III. APPLICATION TO SLAB GEOMETRY

We consider now the slab of Sec. II for the case that the net applied current flows only in the z direction. That is, the average current density components obey $\bar{J}_z > 0$ and $\bar{J}_y = 0$. We assume that a magnetic field $\mathbf{B}_0 = B_0\hat{\mathbf{a}}_0$ is applied parallel to the slab, where $B_0 = |\mathbf{B}_0|$ and $\hat{\mathbf{a}}_0 = \hat{\mathbf{y}}\sin\alpha_0 + \hat{\mathbf{z}}\cos\alpha_0$. We wish to solve for the distributions of $\mathbf{B}(x)$ and $\mathbf{J}(x)$, the magnitude of the average critical-current density $\bar{J}_z = J_c$, and the direction $\psi_E = \alpha_0 + \delta\psi_E$ of the electric field $\mathbf{E} = E_0\hat{\boldsymbol{\psi}}_E$ ($\hat{\boldsymbol{\psi}}_E = \hat{\mathbf{y}}\sin\psi_E + \hat{\mathbf{z}}\cos\psi_E$) as a function of the angle α_0 of the applied field.

We define $\delta B = B - B_0$ and $\delta\alpha = \alpha - \alpha_0$. Then, with the definition $B_I = \mu_0 \bar{J}_z X/2$, we have to first order in B_I (since B_I obeys $B_I \ll B_0$)

$$\delta B_{s0} = B_{s0} - B_0 = -B_I \sin\alpha_0 , \tag{11}$$

$$\delta B_{sX} = B_{sX} - B_0 = B_I \sin\alpha_0 , \tag{12}$$

$$\delta\alpha_{s0} = \alpha_{s0} - \alpha_0 = -(B_I/B_0)\cos\alpha_0 , \tag{13}$$

$$\delta\alpha_{sX} = \alpha_{sX} - \alpha_0 = (B_I/B_0)\cos\alpha_0 . \tag{14}$$

We further define $k_{c\parallel} = \mu_0 J_{c\parallel}/B_0$ and $\mu = k_{c\parallel}X/2$.

Depending upon the angle α_0, the average critical-current density $\bar{J}_z = J_c$ is reached when either (a) B achieves a constant, critical slope across the slab, such that $|J_{\perp}| = J_{c\perp}$, or (b) α achieves a constant, critical slope across the slab, such that $|J_{\parallel}| = J_{c\parallel}$. When condition (a) applies, we can say that flux pinning dominates J_c. From Eqs. (6), (11), and (12) we then obtain

$$J_c = J_{c\perp}/|\sin\alpha_0| . \tag{15}$$

When condition (b) applies, we can say that flux-line cutting dominates J_c. From Eqs. (5), (13), and (14) we then obtain

$$J_c = J_{c\parallel}/|\cos\alpha_0| . \tag{16}$$

Flux pinning [condition (a)] dominates J_c when $\mathbf{B}_0$ is roughly perpendicular to the current direction, while flux-line cutting [condition (b)] dominates when $\mathbf{B}_0$ is roughly parallel (or antiparallel) to the current direction. The two conditions coincide at the four angles α_0 obeying

$$|\tan\alpha_0| = \tan\alpha_c \equiv J_{c\perp}/J_{c\parallel} , \tag{17}$$

i.e., $\alpha_0 = \alpha_c$, $-\alpha_c$, $\pi-\alpha_c$, and $-\pi+\alpha_c$. At these angles both B and α have constant critical slopes across the slab. The B gradient then carries a current density of magnitude $J_{c\perp}$, while the α gradient carries a current density of magnitude $J_{c\parallel}$ but in a direction perpendicular to that of $J_{c\perp}$. The net critical current at the angles $\pm\alpha_c$ and $\pm(\pi-\alpha_c)$ is found from Eqs. (15), (16), and (17) to be

$$J_c = J_{cm} \equiv (J_{c\perp}^2 + J_{c\parallel}^2)^{1/2} . \tag{18}$$

Figure 1(a) shows a sketch of the predicted behavior of J_c as a function of α_0. A polar plot of J_c versus α_0 would yield a rectangle of length $2J_{c\parallel}$ and width $2J_{c\perp}$.

Table I presents the solutions for the physical quantities of interest for arbitrary values of the field angle α_0. Figure 2 exhibits sketches of the profiles of B and α versus x at J_c for the series of equally spaced α_0 values shown in Fig. 3. To bring out the key features of these results, we now focus our attention on just two sets of profiles, curves j and l in Fig. 2.

Curves j show the $B(x)$ and $\alpha(x)$ profiles for α_0 in the range $0 < \alpha_0 < \alpha_c$, where flux-line cutting dominates the critical current and $J_c = J_{c\parallel}/\cos\alpha_0$. Since $B_I = B_0\mu/\cos\alpha_0$ at J_c, where $\mu = k_{c\parallel}x_m = \mu_0 J_{c\parallel}x_m/B_0 \ll 1$, we have from Eqs. (11)–(14), $\delta B_{s0}/B_0 = -\mu\tan\alpha_0$, $\delta B_{sX}/B_0 = \mu\tan\alpha_0$, $\delta\alpha_{s0} = -\mu$, and $\delta\alpha_{sX} = \mu$. The α profile has positive criti-

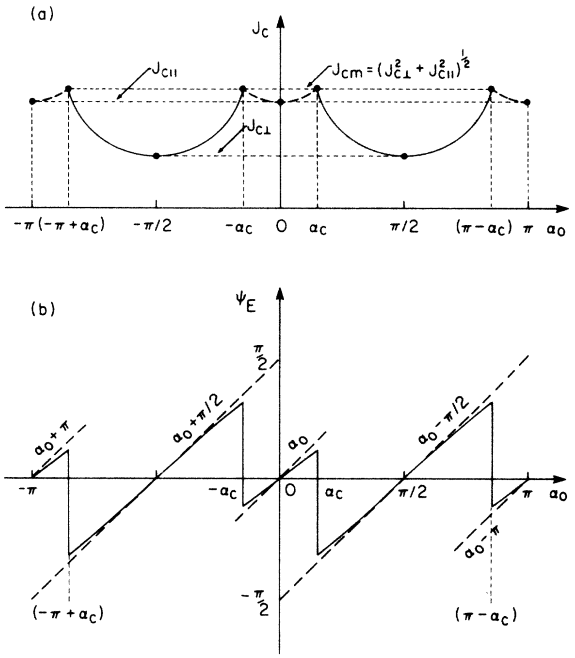

FIG. 1. (a) Sketch of the critical-current density J_c (at the onset of a steady-state electric field) versus the angle α_0 of the applied magnetic field $\mathbf{B}_0$ relative to the current direction for slab geometry. Flux pinning dominates the critical current (solid curves, $J_c=J_{c\perp}/|\sin\alpha_0|$) when $|\tan\alpha_0|>\tan\alpha_c \equiv J_{c\perp}/J_{c\parallel}$, and flux-line cutting dominates (dashed curves, $J_c=J_{c\parallel}/|\cos\alpha_0|$) when $|\tan\alpha_0|<\tan\alpha_c$. (b) Sketch of the electric field angle ψ_E relative to the current direction versus applied field angle α_0 for slab geometry. The behavior is illustrated here for $J_{c\parallel}=2J_{c\perp}$ (or $\alpha_c=0.46$ rad) and $\mu=0.10$ rad.

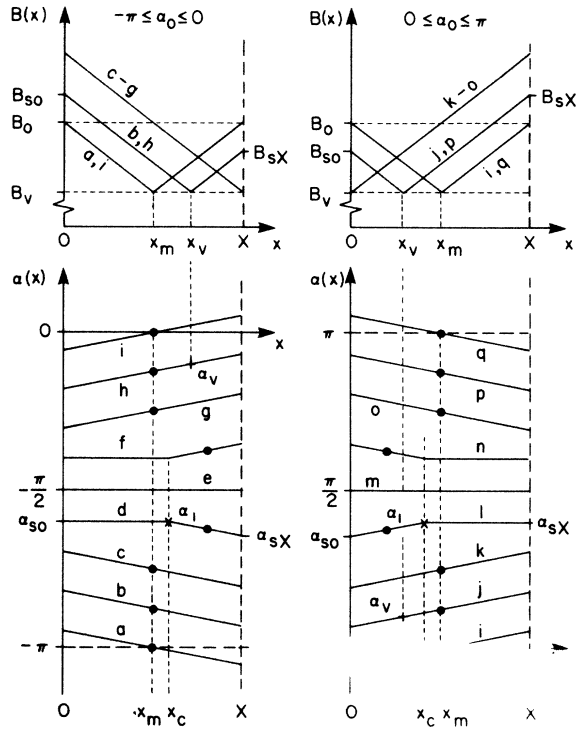

FIG. 2. Profiles of $B(x)$ and $\alpha(x)$ versus x for the equally spaced field angles α_0 labeled in Fig. 3. Left side: $-\pi\le\alpha_0\le 0$; right side: $0\le\alpha_0\le\pi$. B_{s0} and B_{sX} are labeled for curves b, h, j, and p; α_{s0} and α_{sX} are labeled for curves d and l. Also shown are α_0 for all curves (●), α_v for curves h and j (+), and α_1 for curves d and l (×). Here, $\mu=0.17$ rad and $J_{c\parallel}=J_{c\perp}$ ($\alpha_c=\pi/4$). Profiles are calculated only to first order in B_I. See Eqs. (11)–(14).

cal slope for all x, such that

$$\alpha(x)=\alpha_{s0}+k_{c\parallel}x \ . \tag{19}$$

The B profile has negative critical slope to the left of the V-shaped minimum at $x=x_v$, where

$$x_v=(X/2)(1-\tan\alpha_0/\tan\alpha_c) \ , \tag{20}$$

and has positive critical slope to the right of the minimum:

$$B(x)=\begin{cases} B_{s0}-\mu_0 J_{c\perp}x, & 0\le x\le x_v \quad (21a) \\ B_{sX}+\mu_0 J_{c\perp}(x-X), & x_v\le x\le X \ . \quad (21b) \end{cases}$$

At the minimum,

$$B(x_v)=B_v=B_0(1-\mu\tan\alpha_c) \tag{22}$$

and

$$\alpha(x_v)=\alpha_v=\alpha_0-\mu\tan\alpha_0/\tan\alpha_c \ . \tag{23}$$

Both the perpendicular and parallel components of $\mathbf{J}$ are at their critical values: $J_{\parallel}=J_{c\parallel}$ [Eq. (5)] for all x, but $J_{\perp}$ [Eq. (6)] obeys

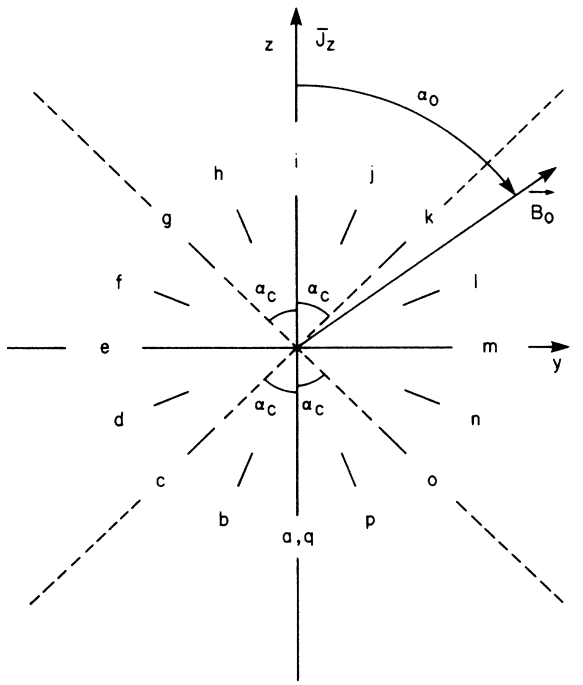

FIG. 3. Key to the equally spaced field angles α_0 examined in Fig. 2. Here, $J_{c\parallel}=J_{c\perp}$ ($\alpha_c=\pi/4$). For example, $\alpha_0=\pi/8$ for j.

TABLE I. Solutions at the critical current for slab geometry ($\bar{J}_z > 0$ and $\bar{J}_y = 0$) as a function of the field angle α_0. Where the symbol $\pm$ appears, the upper sign holds when $\alpha_c < |\alpha_0| < \pi/2$, and the lower sign holds when $\pi/2 < |\alpha_0| < \pi - \alpha_c$. Here, $\alpha_c = \tan^{-1}(J_{c\perp}/J_{c\parallel})$, $k_{c\parallel} = \mu_0 J_{c\parallel}/B_0$, and $\mu = k_{c\parallel} X/2 \ll 1$. NA = not applicable. The behavior for $\pi - \alpha_c < \alpha_0 < \pi$ is equivalent to that for $-\pi - \alpha_c < \alpha_0 < -\pi$.

Quantity	$-\pi-\alpha_c<\alpha_0<-\pi+\alpha_c$	$-\pi+\alpha_c<\alpha_0<-\alpha_c$	$-\alpha_c<\alpha_0<\alpha_c$	$\alpha_c<\alpha_0<\pi-\alpha_c$
Dominant mechanism	Flux-line cutting	Flux pinning	Flux-line cutting	Flux pinning
$J_z = J_c$	$J_{c\parallel}/\lvert\cos\alpha_0\rvert$	$J_{c\perp}/\lvert\sin\alpha_0\rvert$	$J_{c\parallel}/\cos\alpha_0$	$J_{c\perp}/\sin\alpha_0$
$\delta B_{s0}/B_0$	$\mu\tan\alpha_0$	$\mu\tan\alpha_c$	$-\mu\tan\alpha_0$	$-\mu\tan\alpha_c$
$\delta B_{sX}/B_0$	$-\mu\tan\alpha_0$	$-\mu\tan\alpha_c$	$\mu\tan\alpha_0$	$\mu\tan\alpha_c$
$\delta\alpha_{s0}$	μ	$\mu\dfrac{\cot\alpha_0}{\cot\alpha_c}$	$-\mu$	$-\mu\dfrac{\cot\alpha_0}{\cot\alpha_c}$
$\delta\alpha_{sX}$	$-\mu$	$-\mu\dfrac{\cot\alpha_0}{\cot\alpha_c}$	μ	$\mu\dfrac{\cot\alpha_0}{\cot\alpha_c}$
$B(x)$	$B_{s0}-\mu_0 J_{c\perp}x$, $0\le x\le x_v$; $B_{sX}+\mu_0 J_{c\perp}(x-X)$, $x_v\le x\le X$	$B_{s0}-\mu_0 J_{c\perp}x$	$B_{s0}-\mu_0 J_{c\perp}x$, $0\le x\le x_v$; $B_{sX}+\mu_0 J_{c\perp}(x-X)$, $x_v\le x\le X$	$B_{s0}+\mu_0 J_{c\perp}x$
$\alpha(x)$	$\alpha_{s0}-k_{c\parallel}x$	$\alpha_{s0}, 0\le x\le x_c$; $\alpha_{sX}\pm k_{c\parallel}(x-X)$, $x_c\le x\le X$	$\alpha_{s0}+k_{c\parallel}x$	$\alpha_{s0}\pm k_{c\parallel}x$, $0\le x\le x_c$; α_{sX}, $x_c\le x\le X$
x_v/X	$\dfrac{1}{2}\left[1+\dfrac{\tan\alpha_0}{\tan\alpha_c}\right]$	NA	$\dfrac{1}{2}\left[1-\dfrac{\tan\alpha_0}{\tan\alpha_c}\right]$	NA
$\delta B_v/B_0$	$-\mu\tan\alpha_c$	NA	$-\mu\tan\alpha_c$	NA
δa_v	$-\mu\dfrac{\tan\alpha_0}{\tan\alpha_c}$	NA	$-\mu\dfrac{\tan\alpha_0}{\tan\alpha_c}$	NA
x_c/X	NA	$1-\dfrac{\lvert\cot\alpha_0\rvert}{\cot\alpha_c}$	NA	$\dfrac{\lvert\cot\alpha_0\rvert}{\cot\alpha_c}$
α_1	NA	α_{s0}	NA	α_{sX}
Zones	(C_-T_+/C_-T_-)	$(T_+/C_\pm T_+)$	(C_+T_+/C_+T_-)	$(C_\pm T_-/T_-)$
$E_\parallel(x)$	$-E_0\cos(\alpha-\alpha_v)$	0, $0\le x\le x_c$; $E_0\sin(\alpha-\alpha_1)$, $x_c\le x\le X$	$E_0\cos(\alpha-\alpha_v)$	$-E_0\sin(\alpha-\alpha_1)$, $0\le x\le x_c$; 0, $x_c\le x\le X$
$E_\perp(x)$	$E_0\sin(\alpha-\alpha_v)$	E_0, $0\le x\le x_c$; $E_0\cos(\alpha-\alpha_1)$, $x_c\le x\le X$	$-E_0\sin(\alpha-\alpha_v)$	$-E_0\cos(\alpha-\alpha_1)$, $0\le x\le x_c$; E_0, $x_c\le x\le X$
$J_\parallel(x)$	$-J_{c\parallel}$	0, $0<x<x_c$; $\pm J_{c\parallel}$, $x_c<x<X$	$J_{c\parallel}$	$\pm J_{c\parallel}$, $0<x<x_c$; 0, $x_c<x<X$
$J_\perp(x)$	$J_{c\perp}$, $0<x<x_v$; $-J_{c\perp}$, $x_v<x<X$	$J_{c\perp}$	$J_{c\perp}$, $0<x<x_v$; $-J_{c\perp}$, $x_v<x<X$	$-J_{c\perp}$
$\delta\psi_E$	$-\mu\dfrac{\tan\alpha_0}{\tan\alpha_c}+\pi$	$\mu\dfrac{\cot\alpha_0}{\cot\alpha_c}+\dfrac{\pi}{2}$	$-\mu\dfrac{\tan\alpha_0}{\tan\alpha_c}$	$\mu\dfrac{\cot\alpha_0}{\cot\alpha_c}-\dfrac{\pi}{2}$

$$J_\perp = \begin{cases} J_{c\perp}, & 0\le x<x_v \quad (24a) \\ -J_{c\perp}, & x_v<x\le X\,. \quad (24b) \end{cases}$$

The electric field components $E_\parallel$ and $E_\perp$ [Eqs. (7) and (8)] are

$$E_\parallel = E_0\cos(\alpha-\alpha_v)\,, \quad (25)$$

$$E_\perp = -E_0\sin(\alpha-\alpha_v)\,. \quad (26)$$

In the lab coordinate system the macroscopic electric field is constant, $\mathbf{E}=E_0\hat{\boldsymbol{\psi}}_E$, where $\hat{\boldsymbol{\psi}}_E=\hat{\boldsymbol{\alpha}}_V$ and $\psi_E=\alpha_v$.

Flux-line cutting occurs with $E_{||}>0$ for all x. Flux transport also occurs for all x but with $E_{\perp}>0$ where $0<x<x_v$ (a C_+T_+ zone) and with $E_{\perp}<0$ where $x_v<x<X$ (a C_+T_- zone). We thus characterize the zone structure across the slab from left to right as (C_+T_+/C_+T_-), where the subscript to C (T) denotes the sign of the electric field component $E_{||}$ ($E_{\perp}$). Note that, although transport to the right occurs to the left of x_v and transport to the left occurs to the right of x_v, flux-line-cutting B consumption[18] occurs at just the rate needed to make $\partial B/\partial t=0$. Behavior similar to that described here occurs for all field angles in the ranges $-\alpha_c<\alpha_0<\alpha_c$, $-\pi\leqq\alpha_0<-\pi+\alpha_c$, and $\pi-\alpha_c<\alpha_0\leqq\pi$ for which flux-line cutting dominates the critical current. The details are given in Table I.

Curves l in Fig. 2 illustrate qualitatively different behavior of the $B(x)$ and $\alpha(x)$ profiles in the range $\alpha_c<\alpha_0<\pi-\alpha_c$, where flux pinning dominates the critical current and $J_c=J_{c\perp}/\sin\alpha_0$. Since $B_I=\mu_0 B_0\tan\alpha_c/\sin\alpha_0$, we have from Eqs. (11)–(14), $\delta B_{s0}/B_0=-\mu\tan\alpha_c$, $\delta B_{sX}/B_0=\mu\tan\alpha_c$, $\delta\alpha_{s0}=-\mu\cot\alpha_0/\cot\alpha_c$, and $\delta\alpha_{sX}=\mu\cot\alpha_0/\cot\alpha_c$. The B profile has positive critical slope for all x, such that

$$B(X)=B_{s0}+\mu_0 J_{c\perp}x \ . \tag{27}$$

The α profile has positive critical slope only to the left of $x=x_c$, where

$$x_c=X\,|\cot\alpha_0|\,/\cot\alpha_c \ , \tag{28}$$

but is constant to the right of x_c:

$$\alpha(x)=\begin{cases}\alpha_{s0}+k_{c||}x, & 0\leqq x\leqq x_c \quad (29a)\\ \alpha_{sX}, & x_c\leqq x\leqq X \ . \quad (29b)\end{cases}$$

Note that here $\alpha(x_c)=\alpha_1=\alpha_{sX}$. Although $J_{\perp}$ is at its critical value ($J_{\perp}=-J_{c\perp}$) for all x, $J_{||}$ is critical only to the left of x_c:

$$J_{||}=\begin{cases}J_{c||}, & 0\leqq x<x_c \quad (30a)\\ 0, & x_c<x\leqq X \ . \quad (30b)\end{cases}$$

The electric field components $E_{||}$ and $E_{\perp}$ [Eqs. (7) and (8)] thus obey

$$E_{||}=\begin{cases}-E_0\sin(\alpha-\alpha_1), & 0\leqq x\leqq x_c \quad (31a)\\ 0, & x_c\leqq x\leqq X \quad (31b)\end{cases}$$

$$E_{\perp}=\begin{cases}-E_0\cos(\alpha-\alpha_1), & 0\leqq x\leqq x_c \quad (32a)\\ -E_0, & x_c\leqq x\leqq X \ . \quad (32b)\end{cases}$$

Vortices nucleate at the surface $x=X$ with angle α_{sX}. They then move in the $-x$ direction across the T_- zone under the influence of the Lorentz force. They preserve their orientations relative to the specimen until they enter the C_+T_- zone at $x=x_c$. The angle of the electric field, $\psi_E=\alpha_{sX}-\pi/2$, can be obtained from $\mathbf{E}=\mathbf{B}\times\mathbf{v}$. Although this expression does not apply where flux-line cutting is occurring, it is valid in the T_- zone ($x_c<x\leqq X$). Behavior similar to that described above occurs for all field angles obeying $\alpha_c<|\alpha_0|<\pi-\alpha_c$ (see Table I). The angles $\alpha_0=\pm\pi/2$, however, are special, because they are the only two angles for which the CT zone shrinks to zero thickness and the T zone spans the entire cross section.

Figure 1(b) exhibits the predicted electric field angle ψ_E versus the applied magnetic field angle α_0. Just at the critical current we predict a sharp change in the direction of $\mathbf{E}$ by almost 90° at the angles $\pm\alpha_c$ and $\pm(\pi-\alpha_c)$, which separate regions of flux-pinning dominance and flux-line-cutting dominance. At higher currents, ψ_E varies more smoothly with α_0 near $\pm\alpha_c$ and $\pm(\pi-\alpha_c)$.

In this section, we have considered the critical behavior of an infinite slab when a magnetic field is applied parallel to the surface and a current is applied in the z direction. Our results also should apply to good approximation near the middle of a finite strip of thickness X, width Y (sides at $y=0$ and $y=Y$), and length $Z>Y$ (ends at $z=0$ and $z=Z$), provided $X\ll Y$. Our results also should apply not too close to the edges or ends of a thin cylindrical shell of thickness X, radius $R\gg X$, and length $Z>2\pi R$. The shell should have a longitudinal slit along its entire length to permit a longitudinal applied field to freely enter the space inside the cylinder and to prevent any persistent azimuthal currents. Either a current-carrying wire along the axis or a long toroidal field coil with many turns could be used to apply an azimuthal field to the cylindrical shell. Experiments on Nb_3Sn (Refs. 67 and 68), $Pb_{0.90}Tl_{0.10}$ (Ref. 69), and recrystallized NbTi (Ref. 70) have yielded results for J_c versus α_0 similar to those of Fig. 1(a), but apparently no measurements of the direction of $\mathbf{E}$ have been reported in the literature.

IV. APPLICATION TO CYLINDRICAL SHELL GEOMETRY

We consider the experimental arrangement sketched in Fig. 4: a cylindrical shell of inner radius R_i and outer radius $R_0=R_i+X$, where $X\ll R_i$. The outer surface is subjected to a longitudinal applied field $H_z(R_0)=H_a$, and the inner surface to an azimuthal applied field $H_\phi(R_i)=I_w/2\pi R_i$, where I_w is the current in the z direction along a wire on the cylinder axis. (Alternatively, this azimuthal field could be generated by a long coaxial toroidal field coil.) A current I_z is applied to the cylindrical shell, such that the azimuthal field on the outer surface is $H_\phi(R_0)=(I_w+I_z)/2\pi R_0$. We wish to solve for the distributions of $\mathbf{B}(x)$ and $\mathbf{J}(x)$, the magnitude of the average current density $\bar{J}_z=J_c$ at the critical current, and the longitudinal magnetic field inside the shell $H_z(R_i)$ as a function of the angle $\alpha_0=\tan^{-1}[H_\phi(R_i)/H_z(R_0)]$ of the net field applied via I_w and H_a. Since the shell thickness X is much smaller than the average cylinder radius $\bar{R}=(R_i+R_0)/2$, we can safely use the slab geometry introduced in Sec. II, provided we treat the boundary conditions carefully. We align the z axis along the cylinder axis and the x axis in the outward radial direction, such that the y axis points in the azimuthal direction. The coordinates $x=0$ and X correspond to the inner and outer surfaces. The slab boundary conditions become

$$B_{s0y}=\mu_0 I_w/2\pi\bar{R} \ , \tag{33}$$

$$B_{sXz}=\mu_0 H_a \ . \tag{34}$$

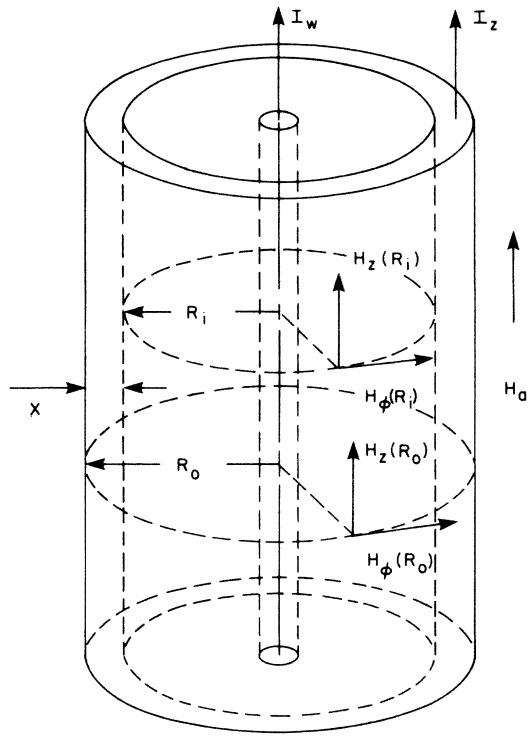

FIG. 4. Sketch of the cylindrical shell geometry considered in Sec. IV. The shell thickness X is greatly exaggerated.

Equations (3) and (4) then relate B_{sXy} to $\bar{J}_z = I_z/2\pi\bar{R}X$ and B_{s0z} to the average induced azimuthal current density $\bar{J}_y$. By analogy with our treatment in Sec. III, we regard the applied magnetic field as $\mathbf{B}_0 = B_{s0y}\hat{\mathbf{y}} + B_{sXz}\hat{\mathbf{z}} = B_0\hat{\boldsymbol{\alpha}}_0$, where $\hat{\boldsymbol{\alpha}}_{s0} = \hat{\mathbf{y}}\sin\alpha_0 + \hat{\mathbf{z}}\cos\alpha_0$.

As in Sec. III, we assume that at the critical current of the shell $|\Delta B_y| \ll B_0$ and $|\Delta B_z| \ll B_0$, such that to first order in $\bar{J}_z$ and $\bar{J}_y$,

$$\delta B_{s0} = B_{s0} - B_0 = \mu_0 \bar{J}_y X \cos\alpha_0 , \tag{35}$$

$$\delta B_{sX} = B_{sX} - B_0 = \mu_0 \bar{J}_z X \sin\alpha_0 , \tag{36}$$

$$\delta\alpha_{s0} = \alpha_{s0} - \alpha_0 = -(\mu_0 \bar{J}_y X/B_0)\sin\alpha_0 , \tag{37}$$

$$\delta\alpha_{sX} = \alpha_{sX} - \alpha_0 = (\mu_0 \bar{J}_z X/B_0)\cos\alpha_0 . \tag{38}$$

In steady state, just above the critical current, Faraday's law requires that $E_y = 0$, such that $\mathbf{E} = E_0\hat{\mathbf{z}}$, $E_{||} = E_0\cos\alpha$, and $E_\perp = -E_0\sin\alpha$.

For α_0 not too close to 0, $\pm\pi/2$, or $\pm\pi$, the behavior of $B(x)$ and $\alpha(x)$ at the critical current is very simple. Both B and α develop constant, critical slopes across the slab, such that $|J_\perp| = J_{c\perp}$, $|J_{||}| = J_{c||}$, and $\mathbf{J}$ has magnitude $J_{cm} = (J_{c\perp}^2 + J_{c||}^2)^{1/2}$. The dependence of $\bar{J}_z = J_c$, given in Table II, is plotted in Fig. 5 as the solid curves. The current density $\mathbf{J}$ (of magnitude J_{cm}) is aligned along the z axis at the four angles $\alpha_0 = \pm\alpha_c$ and $\pm(\pi - \alpha_c)$. For other angles, $\mathbf{J}$ still has the magnitude J_{cm} but is oriented at angle α_c (or $\pi - \alpha_c$) relative to α_0, such that $\bar{J}_y \neq 0$. The behavior of $\bar{J}_y$ versus α_0 is shown by the dashed curves in Fig. 5. In the cylindrical shell geometry of Fig. 4, $\bar{J}_y$ corresponds to an azimuthal current, which because of Eq. (4) makes the internal longitudinal field different from the applied longitudinal field. For $0 < \alpha_0 < \pi$, we have $\Delta B = B_{sX} - B_{s0} > 0$ and a tendency for flux to be transported inward from the outer radius R_0 of Fig. 4 and pumped into the hole of radius R_i. For $-\pi < \alpha_0 < 0$, we have $\Delta B < 0$ and the opposite tendency for flux to be pumped out of the hole and transported outward toward the outer radius R_0.

On the scale of Fig. 5, sketched for $\mu \ll 1$, we note that $\bar{J}_y$ exhibits discontinuities at $\alpha_0 = 0$, $\pm\pi/2$, $\pm\pi$. We present further details of the behavior for α_0 near these special angles in Fig. 6, Table III, and the following discussion.

TABLE II. Solutions at the critical current for cylindrical shell geometry ($\mathbf{E} = E_0\hat{\mathbf{z}}$, $E_{||} = E_0\cos\alpha$, $E_\perp = -E_0\sin\alpha$) as a function of the applied field angle α_0. Here, $k_{c||} = \mu_0 J_{c||}/B_0$, $\mu = k_{c||}X/2 \ll 1$, $J_{cm} = (J_{c\perp}^2 + J_{c||}^2)^{1/2}$, $\alpha_c = \tan^{-1}(J_{c\perp}/J_{c||})$, and $\delta = \mu_0 J_{cm} X/B_0 \ll 1$. See Table III for details of behavior near $\alpha_0 = -\pi$, $-\pi/2$, and 0.

Quantity	$-\pi+2\mu < \alpha_0 < -\pi/2-2\mu$	$-\pi/2+2\mu < \alpha_0 < -2\mu$	$0 \leq \alpha_0 < \pi/2$	$\pi/2 < \alpha_0 \leq \pi$
$\bar{J}_z = J_c$	$-J_{cm}\cos(\alpha_0-\alpha_c)$	$J_{cm}\cos(\alpha_0+\alpha_c)$	$J_{cm}\cos(\alpha_0-\alpha_c)$	$-J_{cm}\cos(\alpha_0+\alpha_c)$
$\bar{J}_y$	$-J_{cm}\sin(\alpha_0-\alpha_c)$	$J_{cm}\sin(\alpha_0+\alpha_c)$	$J_{cm}\sin(\alpha_0-\alpha_c)$	$-J_{cm}\sin(\alpha_0+\alpha_c)$
$\delta B_{s0}/B_0$	$-\delta\sin(\alpha_0-\alpha_c)\cos\alpha_0$	$\delta\sin(\alpha_0+\alpha_c)\cos\alpha_0$	$\delta\sin(\alpha_0-\alpha_c)\cos\alpha_0$	$-\delta\sin(\alpha_0+\alpha_c)\cos\alpha_0$
$\delta B_{sX}/B_0$	$-\delta\cos(\alpha_0-\alpha_c)\sin\alpha_0$	$\delta\cos(\alpha_0+\alpha_c)\sin\alpha_0$	$\delta\cos(\alpha_0-\alpha_c)\sin\alpha_0$	$-\delta\cos(\alpha_0+\alpha_c)\sin\alpha_0$
$\Delta B/B_0$	$-\mu_0 J_{c\perp}x/B_0$	$-\mu_0 J_{c\perp}X/B_0$	$\mu_0 J_{c\perp}X/B_0$	$\mu_0 J_{c\perp}X/B_0$
$\Delta B_z/B_0$	$\delta\sin(\alpha_0-\alpha_c)$	$-\delta\sin(\alpha_0+\alpha_c)$	$-\delta\sin(\alpha_0-\alpha_c)$	$\delta\sin(\alpha_0+\alpha_c)$
$\delta\alpha_{s0}$	$\delta\sin(\alpha_0-\alpha_c)\sin\alpha_0$	$-\delta\sin(\alpha_0+\alpha_c)\sin\alpha_0$	$-\delta\sin(\alpha_0-\alpha_c)\sin\alpha_0$	$\delta\sin(\alpha_0+\alpha_c)\sin\alpha_0$
$\delta\alpha_{sX}$	$-\delta\cos(\alpha_0-\alpha_c)\cos\alpha_0$	$\delta\cos(\alpha_0+\alpha_c)\cos\alpha_0$	$\delta\cos(\alpha_0-\alpha_c)\cos\alpha_0$	$-\delta\cos(\alpha_0+\alpha_c)\cos\alpha_0$
$\Delta\alpha$	-2μ	2μ	2μ	-2μ
$B(x)$	$B_{s0}-\mu_0 J_{c\perp}x$	$B_{s0}-\mu_0 J_{c\perp}x$	$B_{s0}+\mu_0 J_{c\perp}x$	$B_{s0}+\mu_0 J_{c\perp}x$
$\alpha(x)$	$\alpha_{s0}-k_{c||}x$	$\alpha_{s0}+k_{c||}x$	$\alpha_{s0}+k_{c||}x$	$\alpha_{s0}-k_{c||}x$
Zones	C_-T_+	C_+T_+	C_+T_-	C_-T_-
$J_{||}(x)$	$-J_{c||}$	$J_{c||}$	$J_{c||}$	$-J_{c||}$
$J_\perp(x)$	$J_{c\perp}$	$J_{c\perp}$	$-J_{c\perp}$	$-J_{c\perp}$

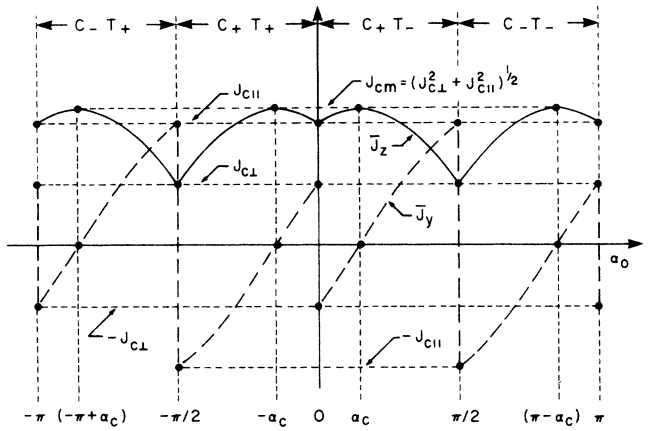

FIG. 5. Sketch of the critical-current density components at the onset of a steady-state electric field versus the angle α_0 of the applied field $\mathbf{B}_0$ relative to the current direction for the cylindrical shell geometry of Fig. 4. Solid curves exhibit the longitudinal critical-current density $J_c=\bar{J}_z$ and dashed curves exhibit the azimuthal current density $\bar{J}_y$. The behavior is illustrated here for $J_{c\parallel}=2J_{c\perp}$ (or $\alpha_c=0.46$ rad) and $\mu \ll 1$ (see Table II).

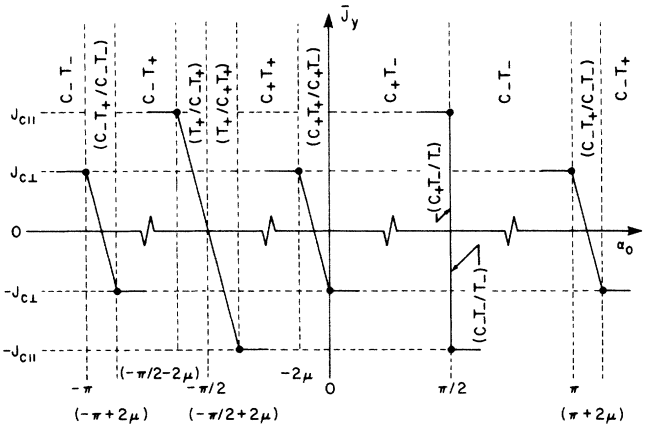

FIG. 6. Sketch of $\bar{J}_y$ at the critical current versus α_0 for α_0 close to $-\pi$, $-\pi/2$, 0, $\pi/2$, and π. The horizontal scale is greatly expanded; $\mu \ll 1$ (see Table III).

A. $\alpha_0 \cong \pi/2$

For α_0 slightly *less* than $\pi/2$, which corresponds to positive values of I_w and $H_\phi(R_i)$ and a very small positive value of $H_z(R_0)$ (see Fig. 4), the field lines at the outer radius take the form of a tightly wound right-handed helix. For an arbitrary initial magnetic state of the cylinder, when the critical value of I_z is reached ($I_z>0$), helical vortices tend to be nucleated at the outer radius and be driven inward by the Lorentz force. Each entering helical vortex increases the longitudinal (z-directed) magnetic flux by one quantum of flux, $\phi_0=h/2e=2.07\times10^{-15}$ Wb. As the vortices reach the inner radius, they contribute to the longitudinal flux in the hole and thereby increase the value of $H_z(R_i)$. This ultimately leads to a positive value of $H_z(R_i)-H_z(R_0)$ and a large and positive value of the azimuthal current density $\bar{J}_y \cong J_{c\parallel}$ (see Figs. 5 and 6). In the final steady state, the rate of increase of B arising from transport is exactly balanced by the rate of decrease of B arising from flux-line-cutting B consumption.[18]

For α_0 slightly *greater* than $\pi/2$, corresponding to a very small *negative* value of $H_z(R_0)$, the field lines at the outer radius of Fig. 4 take the form of a tightly wound *left*-handed helix. Each helical vortex nucleating at the outer radius and migrating into the hole *changes* the longitudinal (z-directed) magnitude flux by ϕ_0. This ultimately leads to a final critical state with a negative value of $H_z(R_i)$ and a large and negative value of the azimuthal current density $\bar{J}_y \cong -J_{c\parallel}$ (see Figs. 5 and 6). The steady-state value of $H_z(R_i)$ is thus very sensitive to the sign of $H_z(R_0)$.

When $\alpha_0=\pi/2$, corresponding to $H_z(R_0)$ precisely equal to zero, $H_z(R_i)$ can have any value in the range $-J_{c\parallel}X \leqq H_z(R_i) \leqq J_{c\parallel}X$. The steady-state zone structure consists of either a C_+T_- zone (when $\bar{J}_y>0$) or a C_-T_- zone (when $\bar{J}_y<0$) next to the inner surface and a T_- zone next to the outer surface (see Fig. 6). In the T_- zone, vortex rings nucleate at the outer radius with angle $\alpha=\pi/2$ and migrate inward until they meet the CT zone, in which α varies linearly from $\pi/2$ to $\tan^{-1}[H_\phi(R_i)/H_z(R_i)]$ at the inner radius.

B. $\alpha_0 \cong -\pi/2$

The details of the behavior when $-\pi/2-2\mu \leqq \alpha_0 \leqq -\pi/2+2\mu$ ($\mu=k_{c\parallel}X/2 \ll 1$ and $k_{c\parallel}=\mu_0 J_{c\parallel}/B_0$), corresponding in Fig. 4 to $I_w<0$, $H_\phi(R_i)<0$, and $|H_z(R_0)| \ll |H_\phi(R_i)|$, are given in Table III. For an arbitrary initial magnetic state of the cylinder, when the critical value of I_z is reached ($I_z>0$), helical vortices tend to be nucleated at the inner radius and be driven outwards by the Lorentz force. Each nucleated helical vortex reduces the magnitude of the longitudinal magnetic flux in the hole by one quantum, ϕ_0. Such flux motion ultimately reduces $H_z(R_i)$ to zero. The final steady-state zone structure consists of a T_+ zone next to the inner surface and either a C_-T_+ zone (when $\bar{J}_y>0$) or a C_+T_+ zone when ($\bar{J}_y<0$) next to the outer surface (see Fig. 6). In the T_+ zone, vortex rings nucleate at the inner radius with angle $\alpha=-\pi/2$ and migrate outward until they meet the CT zone, in which α varies linearly from $-\pi/2$ to $\tan^{-1}[H_\phi(R_0)/H_z(R_0)]$ at the outer radius.

C. $\alpha_0 \cong 0$

The behavior when $-2\mu \leqq \alpha_0 \leqq 0$ corresponds in Fig. 4 to $I_w \leqq 0$, $H_z(R_0)>0$, and $|H_\phi(R_i)| \ll H_z(R_0)$. The critical current is dominated by flux-line cutting throughout the cross section, such that $\bar{J}_z=J_c=J_{c\parallel}$. When $\alpha_0=0$, the B profile is critical with constant slope and with B larger at R_0 than at R_i. When $\alpha_0=-2\mu$, the critical B profile has the opposite slope, such that B is larger at R_i than at R_0. For $-\mu<\alpha_0<0$, however, the critical B profile has a V-shaped minimum similar to that of curve h in Fig. 2. Flux-line-cutting B consumption[18] is

TABLE III. Solutions at the critical current for cylindrical shell geometry ($\mathbf{E}=E_0\hat{\mathbf{z}}$) for applied field angles α_0 near $-\pi$, $-\pi/2$, and 0. Here, $k_{c||}=\mu_0 J_{c||}/B_0$ and $\mu=k_{c||}X/2\ll 1$. The expressions shown in the table are valid to first order in μ. Where the symbol $\pm$ appears, the upper signs holds when $-\pi/2<\alpha_0<-\pi/2+2\mu$, and the lower sign holds when $-2\mu-\pi/2<\alpha_0<-\pi/2$. NA= not applicable.

Quantity	$-\pi\leqq\alpha_0\leqq-\pi+2\mu$	$-\pi/2-2\mu\leqq\alpha_0\leqq-\pi/2+2\mu$	$-2\mu\leqq\alpha_0\leqq 0$
$\bar{J}_z=J_c$	$J_{c\|\|}$	$J_{c\perp}$	$J_{c\|\|}$
$\bar{J}_y$	$-J_{c\perp}(\alpha_0+\pi-\mu)/\mu$	$-J_{c\|\|}(\alpha_0+\pi/2)/2\mu$	$-J_{c\perp}(\alpha_0+\mu)/\mu$
$\delta B_{s0}/B_0$	$(\mu_0 J_{c\perp}X/B_0)(\alpha_0+\pi-\mu)/\mu$	0	$-(\mu_0 J_{c\perp}X/B_0)(\alpha_0+\mu)/\mu$
$\delta B_{sX}/B_0$	0	$-\mu_0 J_{c\perp}X/B_0$	0
$\Delta B/B_0$	$-(\mu_0 J_{c\perp}X/B_0)(\alpha_0+\pi-\mu)/\mu$	$-\mu_0 J_{c\perp}X/B_0$	$(\mu_0 J_{c\perp}X/B_0)(\alpha_0+\mu)/\mu$
$\Delta B_z/B_0$	$(\mu_0 J_{c\perp}X/B_0)(\alpha_0+\pi-\mu)/\mu$	$\alpha_0+\pi/2$	$(\mu_0 J_{c\perp}X/B_0)(\alpha_0+\mu)/\mu$
$\delta\alpha_{s0}$	0	$-(\alpha_0+\pi/2)$	0
$\delta\alpha_{sX}$	-2μ	0	2μ
$\Delta\alpha$	-2μ	$\alpha_0+\pi/2$	2μ
$B(x)$	$B_{s0}-\mu_0 J_{c\perp}x$, $0\leqq x\leqq x_v$; $B_{sX}+\mu_0 J_{c\perp}(x-X)$, $x_v\leqq x\leqq X$	$B_0-\mu_0 J_{c\perp}x$	$B_{s0}-\mu_0 J_{c\perp}x$, $0\leqq x\leqq x_v$; $B_{sX}+\mu_0 J_{c\perp}(x-X)$, $x_v\leqq x\leqq X$
$\alpha(x)$	$\alpha_0-k_{c\|\|}x$	$-\pi/2$, $0\leqq x\leqq x_c$; $-\pi/2\pm k_{c\|\|}(x-x_c)$, $x_c\leqq x\leqq X$	$\alpha_0+k_{c\|\|}x$
x_v or x_c	$x_v/X=(\alpha_0+\pi)/2\mu$	$x_c/X=(1-\lvert\alpha_0+\pi/2\rvert/2\mu)$	$x_v/X=-\alpha_0/2\mu$
α_v	$-\pi$	NA	0
Zones	(C_-T_+/C_-T_-)	$(T_+/C_\pm T_+)$	(C_+T_+/C_+T_-)
$E_{\|\|}(x)$	$-E_0$	0, $0\leqq x\leqq x_c$; $\pm E_0 k_{c\|\|}(x-x_c)$, $x_c\leqq x\leqq X$	E_0
$E_\perp(x)$	$E_0 k_{c\|\|}(x_v-x)$	E_0	$E_0 k_{c\|\|}(x_v-x)$
$J_{\|\|}(x)$	$-J_{c\|\|}$	0, $0\leqq x\leqq x_c$; $\pm J_{c\|\|}$, $x_c<x\leqq X$	$J_{c\|\|}$
$J_\perp(x)$	$J_{c\perp}$, $0\leqq x<x_v$; $-J_{c\perp}$, $x_v<x\leqq X$	$J_{c\perp}$	$J_{c\perp}$, $0\leqq x<x_v$; $-J_{c\perp}$, $x_v<x\leqq X$

responsible for this minimum, which occurs at $x_v=-X\alpha_0/2\mu$, where α_v, the angle of **B**, is zero. $E_\perp$ is zero at x_v but is positive for $x<x_v$ and negative for $x>x_v$. $E_{||}>0$ throughout the cross section. The corresponding $\bar{J}_y$ versus α_0 is sketched in Fig. 6, and further details are given in Table III.

D. $\alpha_0\cong-\pi$

The behavior when $-\pi\leqq\alpha_0\leqq-\pi+2\mu$ corresponds in Fig. 4 to $I_w\leqq 0$, $H_z(R_0)<0$, and $|H_\phi(R_i)|\ll|H_z(R_0)|$. As in the case of $\alpha_0\cong 0$, the critical current is dominated by flux-line cutting. For $-\pi<\alpha_0<-\pi+2\mu$, the critical B profile has a V-shaped minimum similar to that of curve b in Fig. 2. The minimum occurs at $x_v=X(\alpha_0+\pi)/2\mu$, where $\alpha_v=-\pi$. $E_\perp$ is positive for $x<x_v$, negative for $x>x_v$, and zero for $x=x_v$; $E_{||}<0$ throughout the cross section. The corresponding $\bar{J}_y$ versus α_0 is sketched in Fig. 6, and further details are given in Table III.

V. SUMMARY AND DISCUSSION

Flux-line cutting[62,63] has been proposed as a mechanism to explain a variety of phenomena occurring in current-carrying type-II superconductors in parallel magnetic fields. Recently we have incorporated flux-line cutting effects into the usual critical-state theory of flux pinning.[60–62] The result is a macroscopic theory[16–18,36–38] that permits the calculation of the time-dependent hysteretic behavior of type-II superconductors under a wide variety of experimental conditions. The goals of this work have been to provide a framework for quantitative explanations of experimental data and to make predictions for new experiments not yet performed. We hope that such experiments ultimately will be able to demonstrate convincingly whether or not flux-line cutting plays a significant role in the hysteretic magnetic behavior of type-II superconductors.

To set up some stringent tests of the flux-line cutting mechanism, in this paper we have used the macroscopic theory to predict a number of details about the internal magnetic field distribution just above the critical current. We have applied the theory to predict striking behavior in slabs or strips and in thin-walled cylindrical shells. In both cases the critical current is predicted to have maxima when the angle α_0 of the applied field relative to the z direction has the values $\pm\alpha_c$ and $\pm(\pi-\alpha_c)$, where $\alpha_c=\tan^{-1}(J_{c\perp}/J_{c||})$ [Figs. 1(a) and 5]. In the former case, the direction of the electric field is predicted to change by nearly $\pi/2$ at these four angles [Fig. 1(b)]. In the second case, the azimuthal current is predicted to vanish at these four angles but to make large changes in magnitude and sign at the angles $\alpha_0\cong 0$, $\pm\pi/2$, and $\pm\pi$ (Figs. 5 and 6).

Because the above theory assumes that $J_{c\perp}$ and $J_{c||}$ are

isotropic and uniform throughout the specimen, it does not account for the spatially inhomogeneous electric fields that have been observed in several experiments.[9,20] It is possible, however, that incorporating anisotropy and an explicit dependence of $J_{c\perp}$ and $J_{c\parallel}$ upon position might explain these observations. It also would be desirable to extend the theory by introducing surface barriers against entry or exit of magnetic flux and by accounting for the distinction between **B** and $\mu_0\mathbf{H}$ inside the superconductor.

ACKNOWLEDGMENTS

We are grateful to Dr. M. A. R. LeBlanc for stimulating discussions and correspondence. Ames Laboratory is operated for the U.S. Department of Energy by Iowa State University under contract No. W-7405-Eng-82. This work was supported by the Director for Energy Research, Office of Basic Energy Sciences, U.S. Department of Energy.

*Present address: Departamento de Fisica, Universidad Autónoma de Puebla, Apartado Postal J-48, Puebla, Puebla, Mexico.

[1]An excellent review of the literature regarding this problem as of 1974 is given by W. E. Timms and D. G. Walmsley, J. Phys. F **5**, 2897 (1975).

[2]E. H. Brandt, J. Low Temp. Phys. **39**, 41 (1980).

[3]E. H. Brandt, Phys. Lett. **79A**, 207 (1980).

[4]E. H. Brandt, J. Low Temp. Phys. **44**, 33 (1981).

[5]E. H. Brandt, J. Low Temp. Phys. **44**, 59 (1981).

[6]E. H. Brandt, Physica **107B**, 459 (1981).

[7]E. H. Brandt, Phys. Rev. B **25**, 5756 (1982).

[8]A. M. Campbell, Helv. Phys. Acta **53**, 404 (1980).

[9]J. R. Cave and J. E. Evetts, Philos. Mag. B **37**, 111 (1978).

[10]J. R. Cave, J. E. Evetts, and A. M. Campbell, J. Phys. (Paris) Colloq. **39**, C6-614 (1978).

[11]J. R. Clem, Phys. Lett. **54A**, 452 (1975).

[12]J. R. Clem, Phys. Lett. **59A**, 401 (1976).

[13]J. R. Clem, Phys. Rev. Lett. **38**, 1425 (1977).

[14]J. R. Clem, J. Low Temp. Phys. **38**, 353 (1980).

[15]J. R. Clem, Physica **107B**, 453 (1981).

[16]J. R. Clem, Phys. Rev. B **26**, 2463 (1982).

[17]J. R. Clem and A. Perez-Gonzalez, in *Proceedings of the 17th International Conference on Low Temperature Physics LT—17,* edited by U. Eckern, A. Schmid, W. Weber, and H. Wühl (Elsevier, Amsterdam, 1984), p. 583.

[18]J. R. Clem and A. Perez-Gonzalez, Phys. Rev. B **30**, 5041 (1984).

[19]J. R. Clem and S. Yeh, J. Low Temp. Phys. **39**, 173 (1980).

[20]T. Ezaki and F. Irie, J. Phys. Soc. Jpn. **40**, 382 (1976).

[21]T. Ezaki, K. Yamafuji, and F. Irie, J. Phys. Soc. Jpn. **40**, 1271 (1976).

[22]A. Fevrier and J. C. Renard, Adv. Cryog. Eng. **24**, 363 (1977).

[23]F. Irie, T. Ezaki, and K. Yamafuji, IEEE Trans. Magn. **MAG-11**, 332 (1975).

[24]F. Irie, T. Ezaki, and K. Yamafuji, in *International Discussion Meeting on Flux Pinning in Superconductors,* edited by P. Haasen and H. C. Freyhardt (Akademie der Wissenschafte Göttingen, 1975), p. 294.

[25]V. G. Kogan, Phys. Rev. B **21**, 2799 (1980).

[26]V. G. Kogan, Phys. Rev. B **21**, 3027 (1980).

[27]V. G. Kogan, Phys. Lett. **79A**, 337 (1980).

[28]M. A. R. LeBlanc and B. R. Kiggins, Solid State Commun. **8**, 633 (1970).

[29]J. P. Lorrain, M. A. R. LeBlanc, and A. Lachaine, Can. J. Phys. **57**, 1458 (1979).

[30]T. Matsushita, Phys. Lett. **86A**, 123 (1981).

[31]T. Matsushita, Phys. Lett. **96A**, 149 (1983).

[32]T. Matsushita, J. Phys. Soc. Jpn. **54**, 1054 (1985).

[33]T. Matsushita, Y. Hasegawa, and J. Miyake, J. Appl. Phys. **54**, 5277 (1983).

[34]T. Matsushita and F. Irie, J. Phys. Soc. Jpn. **54**, 1066 (1985).

[35]T. Matsushita, S. Ozaki, E. Nishimori, and K. Yamafuji, J. Phys. Soc. Jpn. **54**, 1060 (1985).

[36]A. Perez-Gonzalez and J. R. Clem, Phys. Rev. B **31**, 7048 (1985).

[37]A. Perez-Gonzalez and J. R. Clem, Phys. Rev. B **32**, 2909 (1985).

[38]A. Perez-Gonzalez and J. R. Clem, J. Appl. Phys. **58**, 4326 (1985).

[39]S. Takacs, Phys. Status Solidi A **32**, 485 (1975).

[40]S. Takacs, Czech. J. Phys. B **33**, 208 (1983).

[41]S. Takacs and I. Hlasnik, J. Low Temp. Phys. **54**, 397 (1984).

[42]S. Takacs and A. Pevala, Phys. Status Solidi A **41**, K175 (1977).

[43]W. E. Timms and D. G. Walmsley, J. Phys. F **6**, 2107 (1976).

[44]B. Turck, IEEE Trans. Magn. **MAG-13**, 548 (1977).

[45]D. G. Walmsley and W. E. Timms, J. Phys. F **7**, 2373 (1977).

[46]K. Yamafuji, T. Kawashima, and H. Ichikawa, J. Phys. Soc. Jpn. **39**, 581 (1975).

[47]K. Yamafuji and T. Matsushita, J. Phys. Soc. Jpn. **47**, 1069 (1979).

[48]R. Boyer, Ph.D. thesis, University of Ottawa, Canada (1977).

[49]R. Boyer, G. Fillion, and M. A. R. LeBlanc, J. Appl. Phys. **51**, 1692 (1980).

[50]R. Boyer and M. A. R. LeBlanc, Solid State Commun. **24**, 261 (1977).

[51]J. R. Cave and M. A. R. LeBlanc, J. Appl. Phys. **53**, 1631 (1982).

[52]G. Fillion, R. Gauthier, and M. A. R. LeBlanc, Phys. Rev. Lett. **43**, 86 (1979).

[53]R. Gauthier, Ph.D. thesis, University of Ottawa, Canada (1976).

[54]R. Gauthier and M. A. R. LeBlanc, IEEE Trans. Magn. **MAG-13**, 560 (1977).

[55]A. Lachaine, Ph.D. thesis, University of Ottawa, Canada (1976).

[56]A. Lachaine and M. A. R. LeBlanc, in *Low Temperature Physics LT-13,* edited by K. D. Timmerhaus, W. J. O'Sullivan, and E. F. Hammel (Plenum, New York, 1974), Vol. 3, p. 247.

[57]A. Lachaine and M. A. R. LeBlanc, IEEE Trans. Magn. **MAG-11**, 336 (1975).

[58]A. Lachaine, M. A. R. LeBlanc, and J. P. Lorrain, Physica **107B**, 433 (1981).

[59]M. A. R. LeBlanc and B. C. Belanger, Appl. Phys. Lett. **8**, 291 (1966).

[60]H. London, Phys. Lett. **6**, 162 (1963).

[61]C. P. Bean, Rev. Mod. Phys. **36**, 31 (1964).

[62]A. M. Campbell and J. E. Evetts, Adv. Phys. **21**, 199 (1972).

[63]D. G. Walmsley, J. Phys. F **2**, 510 (1972).

[64]An excellent introduction to magnetic reconnection and a sur-

vey of recent observations and developments can be found in *Magnetic Reconnection in Space and Laboratory Plasmas,* edited by Edward W. Hones, Jr. (American Geophysical Union, Washington, D.C., 1984).
[65]K. W. Schwarz, Phys. Rev. Lett. **49**, 283 (1982).
[66]K. W. Schwarz, Phys. Rev. Lett. **50**, 364 (1983).
[67]G. W. Cullen, G. D. Cody, and J. P. McEvoy, Jr., Phys. Rev. **132**, 577 (1963).
[68]G. W. Cullen and G. D. Cody, J. Appl. Phys. **44**, 2838 (1973).
[69]H. R. Hart, Jr. and P. S. Swartz, Phys. Rev. **156**, 403 (1967).
[70]K. P. Jüngst, IEEE Trans. Magn. **MAG-11**, 340 (1975).